Supporting Information for

Formation of Mercury Sulfide from Hg(II)-Thiolate Complexes in Natural Organic Matter

Alain Manceau,[1] Cyprien Lemouchi,[1,2] Mironel Enescu,[3] Anne-Claire Gaillot,[4] Martine Lanson,[1] Valérie Magnin,[1] Pieter Glatzel,[5] Brett A. Poulin,[6,7] Joseph N. Ryan,[6] George R. Aiken,[7] Isabelle Gautier-Luneau,[2] Kathryn L. Nagy[8]

[1]ISTerre, Université Grenoble Alpes, CNRS, 38000 Grenoble, France.

[2]Institut Néel, Université Grenoble Alpes, CNRS, 38000 Grenoble, France.

[3]Laboratoire Chrono Environnement, Université de Franche-Comté, CNRS, 25030 Besançon, France.

[4]Institut des Matériaux Jean Rouxel (IMN), Université de Nantes, CNRS, 2 Rue de la Houssinière, 44322 Nantes, France.

[5]European Synchrotron Radiation Facility (ESRF), 71 Rue des Martyrs, 38000 Grenoble, France.

[6]Department of Civil, Environmental, and Architectural Engineering, University of Colorado Boulder, 428 UCB, Boulder, Colorado 80309-0428, United States.

[7]U. S. Geological Survey, 3215 Marine Street, Boulder, Colorado 80303, United States.

[8]Department of Earth and Environmental Sciences, MC-186, 845 West Taylor Street, University of Illinois at Chicago, Chicago, Illinois 60607, United States.

Number of pages: 18

Number of Figures: 12

1. Materials and Methods

1.1. Soil samples

Soil samples were collected 1 m from the bank of East Fork Poplar Creek, TN, USA (N 35°57.959; W 84°21.570; ± 7 m) in October, 2010. Soil from the O (0-5 cm depth) and A horizon (20-30 cm) were collected in borosilicate glass jars with Teflon®-lined caps (I-Chem 200 series, Fisher Scientific) and shipped overnight to Boulder, CO, USA. At a depth of 40 cm in the soil column, we observed redoximorphic features of gray clay and orange mottling, both of which indicate an oxic/anoxic redox transition. Both O and A horizon soils were collected above this redox transition. The O horizon contains partly decayed organic matter and the underlying A horizon contains mineral matter mixed with some humus.

Soil samples were air-dried and sieved to < 2 mm using a stainless steel sieve to remove large rocks and organic debris. The total mercury contents of bulk O and A horizon soils were 14.8 and 54.9 mg kg^{-1}, respectively, as determined by thermal desorption and atomic absorption spectroscopy detection (Milestone S.r.l., DMA-80 Direct Mercury Analyzer). The organic matter contents of bulk O and A horizon soils were 79.6 and 38.8 g kg^{-1}, respectively, as determined by loss on ignition (LOI) at 550° C for 2 h. For comparison to the Hg-SOM experiments described in section 1.2.2, the O and A horizons have 186 mg Hg/kg SOM and 1415 mg Hg/kg SOM, respectively. Making an approximate analogy with the Elliot Soil humic acid used in the SOM experiments (with 0.44% sulfur by mass of which 18.4% is thiol sulfur,[1]) the molar ratio of mercury to thiol sulfur is estimated to be ~1:25 in the O horizon and ~1:4 in the A horizon.

Soil fractions were isolated to obtain sufficient concentrations of solid-phase mercury for spectroscopic analysis. The clay-sized (clay) fractions of the two soil horizons were separated using slightly different procedures. O horizon soil was separated into the clay fraction (0.1-2 µm) using centrifugation and filtration. Soil (0.5 g) was added to 50 mL Teflon® centrifuge tubes containing 40 mL Milli-Q water (> 18MΩ cm resistance) for 6 h, sonicated for 2 min to disaggregate minerals, and centrifuged at 1000 rpm for 2 min, removing soil particles > 2 µm assuming a density of 2.65 g cm^{-3}. The suspended clay fraction was collected on a 0.1 µm filter (Supor®, Pall Life Science), rinsed with 10 mL Milli-Q water, gently removed from the wet filter, and dried under N_2. The A horizon soil was separated into silt-sized (silt; 2-63 µm) and clay (< 2 µm) fractions using mechanical sieving and centrifugation. First, A horizon soil was soaked in Milli-Q water for 6 h, sonicated for 2 min to disaggregate minerals, and sieved using a 63 µm stainless steel sieve. Next, the clay fraction was separated from the silt fraction by centrifugation. The solution containing < 63 µm soil was sonicated for 2 min, placed in 50 mL Teflon® tubes, and centrifuged at 1000 rpm for 2 min, removing soil particles > 2 µm assuming a density of 2.65 g cm^{-3}. The silt and clay fractions were dried under air.

The total mercury content was determined on soil fractions by aqua regia digestion (3:1 concentrated trace-metal grade HCl:HNO_3; Fisher Scientific), preservation with 1%

volume/volume (v/v) 0.2 M BrCl, and aqueous analysis using $SnCl_2$ reduction, dual amalgamation, and cold vapor atomic fluorescence spectroscopy (CVAFS) detection following EPA method 1631 (Tekran 2600; method detection limit of 2.5 pM; relative percent deviation between duplicate analyses averaged 0.7%). A horizon samples were analyzed in digestion duplicate. The O horizon sample was analyzed in digestion singlet due to limited sample mass. The total mercury content of the O horizon clay fraction was 47.6 mg kg^{-1}. The total mercury content of A horizon clay and silt fractions were 191 ± 1.8 mg kg^{-1} and 80.7 ± 1.6 mg kg^{-1}, respectively.

1.2. Preparation and characterization of α-HgS, β-HgS and Hg-SOM

1.2.1. α-HgS and β-HgS

Cinnabar was purchased from ABCR GmbH & Co KG and its purity and crystallinity verified by powder X-ray diffraction (XRD). Pure metacinnabar could not be obtained commercially[2] and therefore was synthesized by three different protocols. In the first, Hg(II) was reacted with L-cysteine followed by solvothermal treatment.[3] This synthesized β-HgS is referred to as well crystallized and was used as the reference phase shown in Figures 1C and 2C. In the second, Hg(II) was reacted with L-cysteine ethyl ester (L-Cys-OEt) and the Hg-(L-Cys-OEt)$_2$ complex was aged in the dark in the presence of air at room temperature. The third protocol was the same as the second, except that aging was carried out in the presence of argon. This third synthesis produced the nanoparticulate β-HgS used to fit the soil spectra in Figure 2D.

In the solvothermal synthesis of metacinnabar 500 mg (1.437 mmol) of $Hg(NO_3)_2.H_2O$ (98.5% purity) dissolved in 5 mL methanol was added dropwise to 5 mL of Milli-Q water containing 530.5 mg (4.313 mmol) L-cysteine. A white precipitate formed as Hg(II) was added. The solution with suspended solids was transferred to a 20 mL Teflon®-lined stainless steel autoclave. The autoclave was sealed, heated from 60 to 160 °C at 10°C/h, held at 160 °C for 48 h, and then gradually cooled to 40°C at 12°C/h. The resulting black powder (β-HgS) was separated by centrifugation, washed several times with Milli-Q water and dried at 60°C in an oven for characterization by powder X-ray diffraction, field emission scanning electron microscopy (FESEM), and transmission electron microscopy (TEM). The yield, expressed as the quantity of Hg (mmol) in HgS relative to the initial quantity of Hg(II) (mmol), was 72%. The rest of the Hg remained complexed in the supernatant.

The XRD pattern was collected at room temperature (RT) on a Siemens D5000 diffractometer with the following conditions: $\lambda(CuK_{\alpha 1})$ = 1.54056 Å (40 mA, 40 kV), $10° < 2\theta < 90°$, and 7.5 s counting time per 0.016° 2θ step. The XRD pattern was indexed in the *F*-43m cubic space group in agreement with crystallographic data for β-HgS (Fig. S1A).[4, 5] The unit-cell dimension obtained by whole-pattern fitting (Le Bail method[6]) using the Fullprof program[7] is a = 5.851(2) Å (R_p = 13.5%, R_{wp} = 12.5% and R_{Bragg} = 2.8%). This value coincides with the International Centre for Diffraction Data (ICDD) value (a = 5.85170 Å, n° 00-006-0261) and is close to that reported previously (5.8537 Å).[4] The coherent domain size was estimated to be 80 nm with Scherrer's equation: $D = (0.9\lambda/B \cos\theta)$ where B is the line broadening at full width half maximum (FWHM)

and θ is the diffraction angle. This pure and well-crystallized β-HgS was used as the mercury sulfide model compound for HR-XANES after verifying that its He-T spectrum was distinct from α-HgS.[2] (Fig. S2)

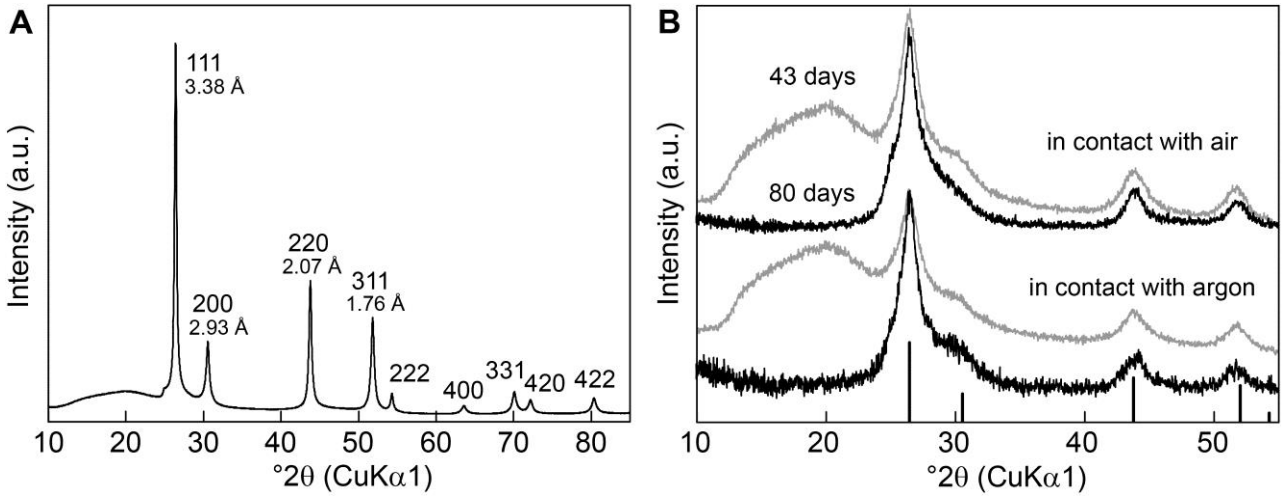

Fig. S1. (A) XRD pattern of solvothermal β-HgS. *hkl* reflections and *d*-spacings of the main peaks are reported. (B) XRD patterns of the black precipitates formed by aging for 43 days (grey lines) and 80 days (black lines) solutions of Hg-(L-Cys-OEt)$_2$ complexes equilibrated with air or argon. The diffraction maxima coincide with those for β-HgS (vertical lines).

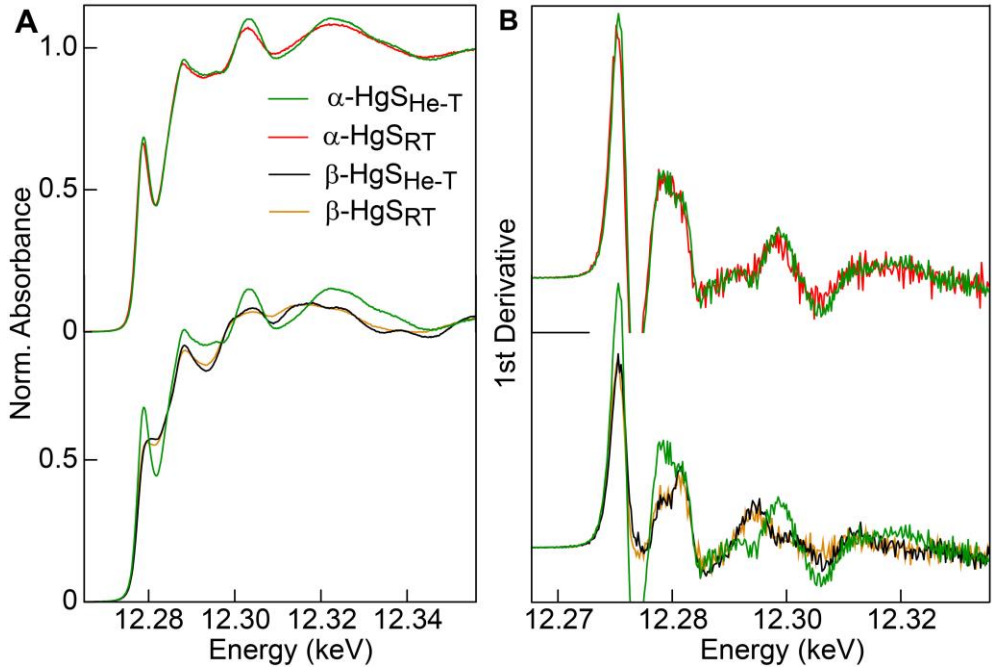

Fig. S2. HR-XANES spectra (A) and 1st derivatives (B) of α-HgS and solvothermal β-HgS at RT and He-T. The spectral features increase when the temperature is lowered, which is explained by a reduction of thermal effects, leading to a better signal definition, and thus more accurate determination of the Hg species. The derivatives of β-HgS are the same at RT and He-T, showing that there is no evidence for the appearance of an α-HgS component at low temperature.

The solvothermal β-HgS grains were examined further using a ZEISS ultra+ FESEM (3.0 kV) and in-lens backscattered secondary electron (BSE) detection. The β-HgS powder was spread on carbon tape and coated with amorphous carbon to prevent charging. The crystals occur as rosette-bundled aggregates 0.5 to 1 μm in diameter and as platelets on the order of 0.5 μm in diameter (Fig. S3).

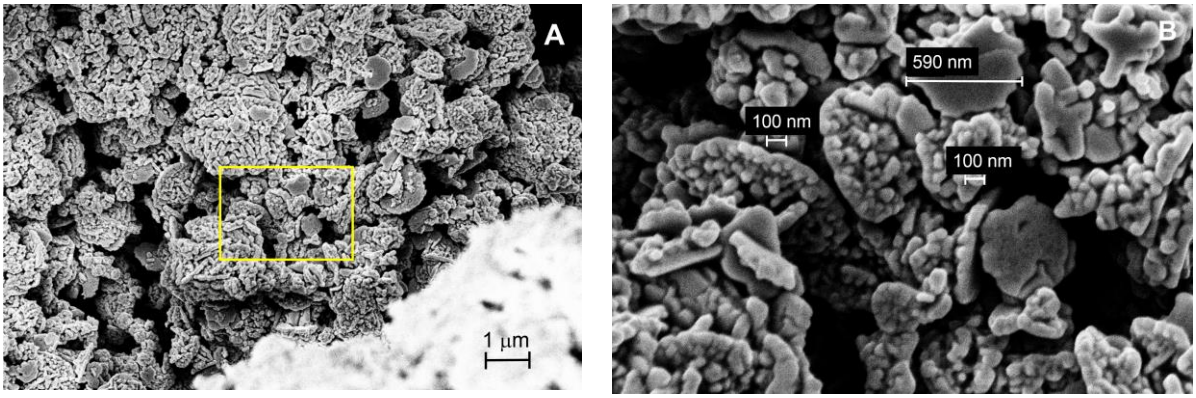

Fig. S3. Secondary electron FESEM images of the solvothermal β-HgS. (A) Low magnification image. (B) High magnification image of the rectangular area shown in A.

The solvothermal β-HgS crystals also were examined using a Philips CM 300 transmission electron microscope equipped with a LaB6 source and operating at 300 kV. Images were recorded with a digital camera (TemCam-F416). The samples were prepared by suspending some powder in ethanol followed by ultrasonic dispersion for 30 min and deposition of a drop of suspension on standard copper grids coated with holey amorphous carbon. The β-HgS crystallites are about ~40 nm wide by 80 nm long (Figs. S4A and S4B). High-resolution TEM images were recorded on a Hitachi H-9000NAR TEM with a LaB6 cathode operated at 300kV and equipped with a Gatan Multiscan charge-coupled device camera. Under high magnification, the β-HgS crystallites appear surrounded by a 2-5 nm thick amorphous layer (Fig. S4E). This layer is observed less distinctly on the rim of the crystallites at medium resolution (Fig. S4B). Atomic resolution images of single grains show well-crystallized domains 20 to 80 nm in diameter, in agreement with the XRD estimate (Fig. S4C). Fast Fourier transforms (Figs. S4C and S4D), and spacing from intensity profiles across atomic columns on the HRTEM images (Fig. S4F), coincide with the cubic structure of β-HgS oriented along <111> (Fig. S4C) and <110> (Fig. S4E) zone axes. The second orientation[3] is most common. Note that β-HgS and α-HgS are more confidently distinguished by X-ray than electron diffraction because the 111 and 200 reflections observed for β-HgS in the common <110> crystal orientation have theoretical *d*-spacings (3.38 Å and 2.93 Å) and relative intensities similar to the 101 and 012 reflections (3.36 Å and 2.86 Å) for α-HgS in the <211> orientation.

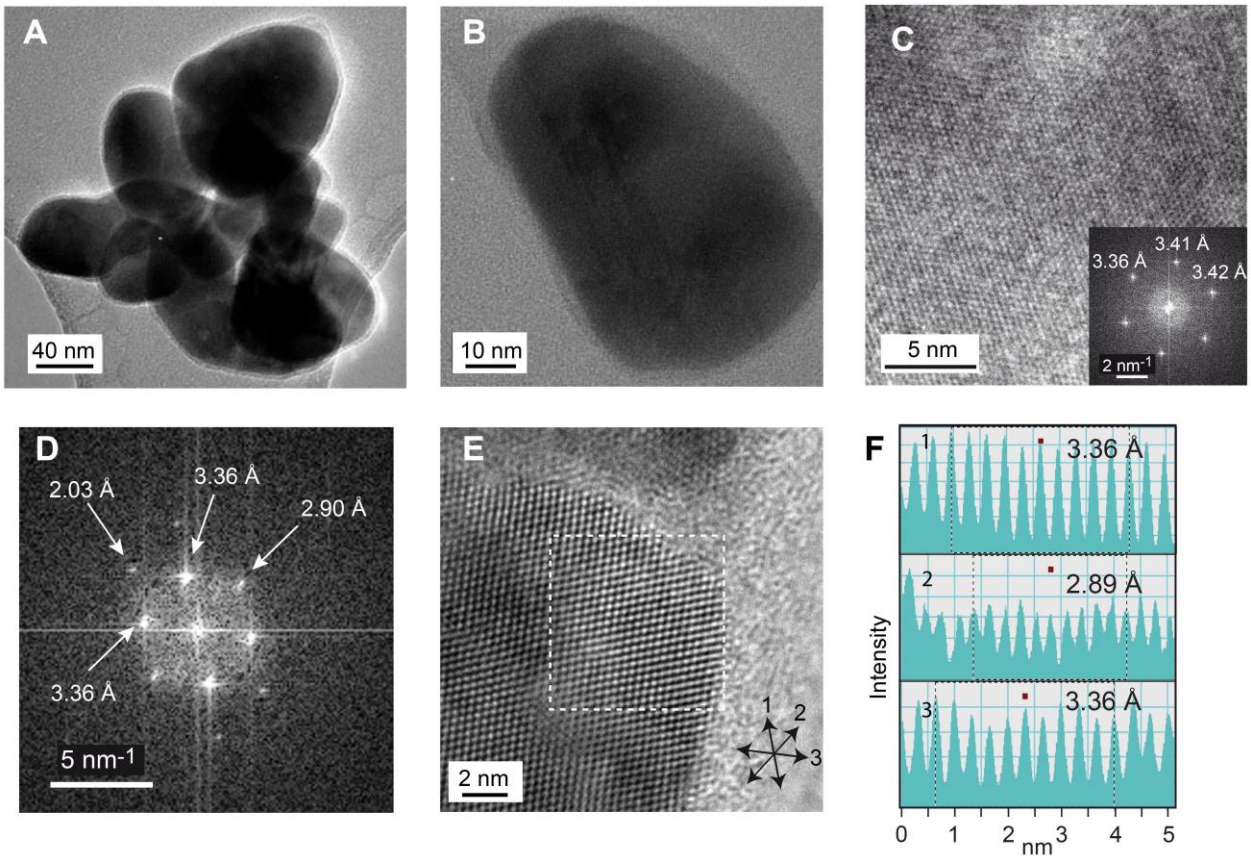

Fig. S4. TEM images of solvothermal β-HgS. (A) Aggregate of crystallites. (B) Single crystallite. (C) HRTEM image and fast Fourier transform (FFT) of β-HgS single crystal viewed along <111> zone axis. (D-F) Atomic resolution image of a single crystal (E) with FFT (D) of the imaged region in the dotted square showing the cubic symmetry of β-HgS oriented along the <110> zone axis, and histogram of intensities (F) across atomic columns from the same region in three directions giving lattice spacings *d*(111) = 3.36 Å and *d*(200) = 2.89-2.90 Å consistent with β–HgS.

The experimental schemes used to synthesize β-HgS from the mixture of Hg(II) and L-Cys-OEt are shown in Figure S5. All glassware and magnetic stir bars were washed with Milli-Q water and pure ethanol, then dried at 150 °C in an oven for 24 h. One mmol (311 mg) *n*$Bu_4NCH_3CO_2$ (Sigma-Aldrich, CAS = 10534-59-5) and one mmol (190 mg) $HSCH_2CH(NH_3)CO_2CH_2CH_3$,Cl (L-Cys-OEt, HCl; L-Cysteine ethyl ester hydrochloride, Sigma-Aldrich, CAS = 868-59-7) powders were degassed separately by four vacuum/argon cycles, then kept under argon until dissolved separately in 10 mL argon-purged Milli-Q water. One half mmol (160 mg) $Hg(CH_3CO_2)_2$ powder (Sigma-Aldrich, cas = 1600-27-7) was conditioned as received in a third argon-purged glass flask and dissolved in 10 mL argon-purged Milli-Q water. The three solutions were further degassed for 10 min under flowing argon while stirring. Then the *n*$Bu_4NCH_3CO_2$ and $Hg(CH_3CO_2)_2$ solutions were mixed and added dropwise to the L-Cys-OEt, HCl solution while stirring continuously. After 15 min, the pH of the mixture was 4.5. The ^1H and ^{13}C NMR spectra for a mixture of 2 molar equivalents of L-Cys-OEt, HCl and 1 molar equivalent of $Hg(CH_3CO_2)_2$ at pH 4.5 show that all ligands are complexed to Hg(II) forming only the $[Hg(SCH_2CH(NH_3)CO_2CH_2CH_3)_2]^{2+}$ linear

complex (Fig. S6). In this complex, Hg atoms are exclusively bonded to two sulfur atoms and not to the amino and carboxyl moieties. Hence, the complex provides the RS-Hg-SR units from which β-HgS is formed. The solution was split into two batches. The headspace of split I (2nd β-HgS synthesis protocol) was filled with air and the flask opened to replace the air every four days. The flask from split II (3rd β-HgS synthesis protocol) was sealed with a rubber septum containing a needle adapter to an argon-filled balloon and the headspace maintained under argon at all times by recycling argon every four days. The two flasks were wrapped with aluminum foil and stored in the dark at 25 °C without stirring for 80 days. The flasks were exposed to the light for no longer than 5 min total to take photographs of the aged solutions (Fig. 3D). Aliquots of the solutions were sampled after 43 and 80 days, centrifuged, rinsed three times with Milli-Q water, and dried in a P_2O_5-containing desiccator. The powder was characterized by XRD ($10° < 2\theta < 55°$, 15 s counting time per 0.026° 2θ step) and HR-XANES. Solids from both experiments showed peaks for poorly crystallized β-HgS (Fig. S1B) and a HR-XANES spectrum nearly identical to the A horizon spectrum (Fig. S7).

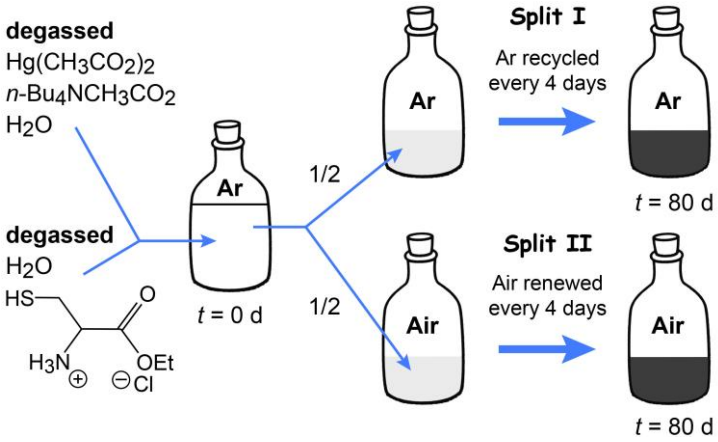

Fig. S5. Experimental schemes for the synthesis of β-HgS from Hg(II) complexed to L-Cys-OEt in solutions equilibrated with air and with argon. The Hg:S:$CH_2CH(NH_3)CO_2CH_2CH_3$ ratio is 1:2:2.

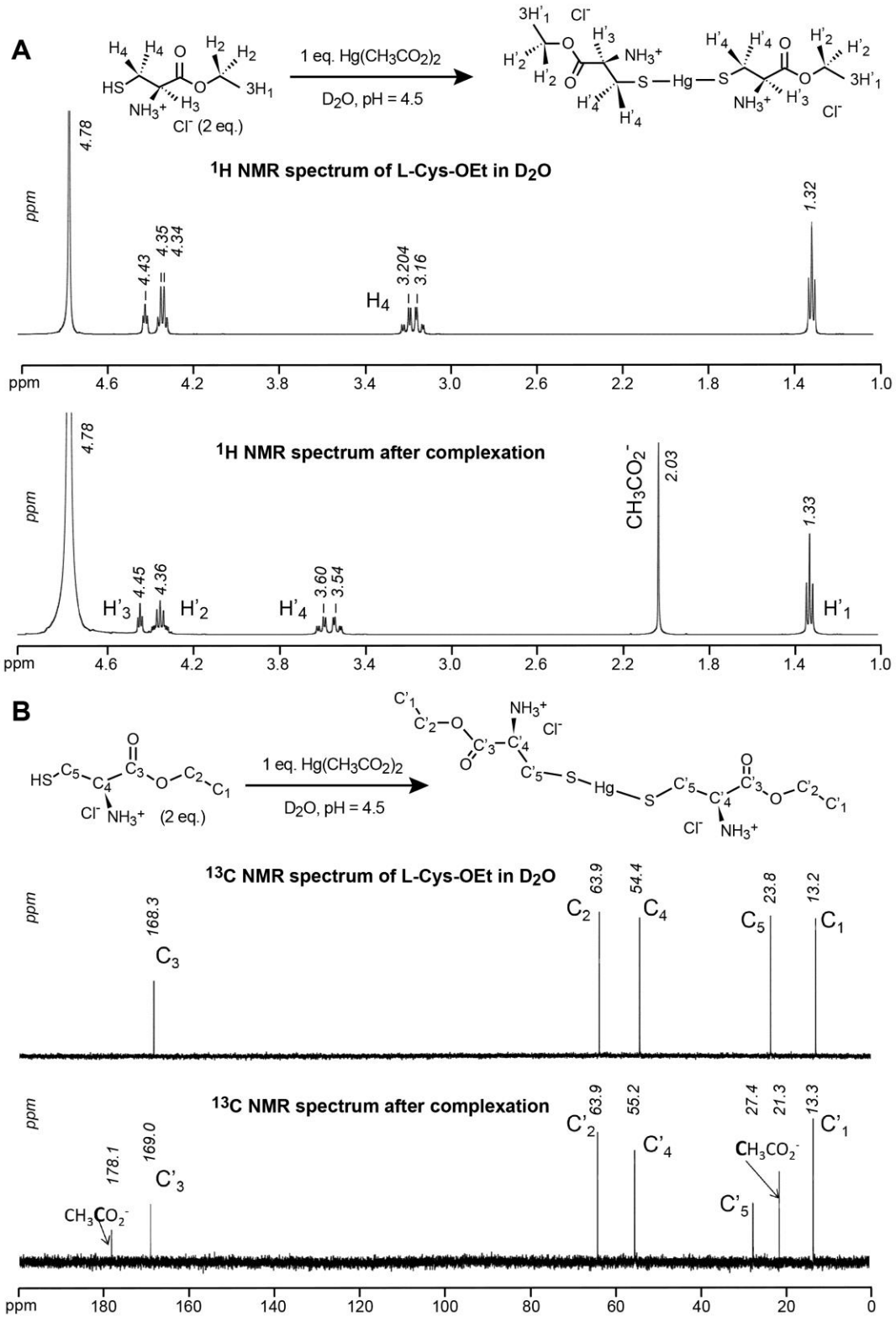

Fig. S6. NMR spectra of L-Cys-OEt in D_2O *(upper part*) and after complexation to Hg(II) (*bottom part*) for ^{1}H (A) and ^{13}C (B) respectively. Upon complexation of L-Cys-OEt to Hg(II) in D_2O solution (pH 4.5), the resonances of the two protons H_4 (A) and carbon C_5 (B) nearest to sulfur (free ligand) are shifted upfield by 0.4 ppm (H'_4) and 3.6 ppm (C'_5), respectively, verifying that all the ligand is complexed to Hg(II) in

$[Hg(SCH_2CH(NH_3)CO_2CH_2CH_3)_2]Cl_2$. These values are in line with those reported in the literature for Hg(II) bonded to cysteinyl sulfur.[8] Experimental conditions were as follows: $Hg(CH_3CO_2)_2$ (32 mg, 0.1 mmol) in 2 mL D_2O was added dropwise to 4 mL L-Cys-OEt, HCl (38 mg, 0.2 mmol) in D_2O. The homogenous mixture was stirred for 15 min, and then, pH was increased from 2.5 to 4.4 with 10^{-2} M KOH in D_2O. NMR data for $[Hg(SCH_2CH(NH_3)CO_2CH_2CH_3)_2]Cl_2$.: ^1H NMR (D_2O, 500 MHz) : δ {ppm} (signal multiplicity : s for singlet, m for multiplet, t for triplet and q for quartet), integration number of labelled H_i) 4.45 (m, 1H'$_3$), 4.36 (q, *J*=7Hz, 2H'$_2$), 3.57 (m, 2H'$_4$), 2.03 (s, 3H ($CH_3CO_2^-$)), 1.33 (t, *J*=7Hz, 3H'$_1$); ^{13}C NMR (D_2O, 500 MHz) : δ {ppm} (labelled C_i) 178.1 (COOH{$CH_3CO_2^-$}, 169.0 (C'$_3$), 63.9 (C'$_2$), 55.2 (C'$_4$), 27.4 (C'$_5$), 21.3 (CH_3{$CH_3CO_2^-$}), 13.3 (C'$_1$).

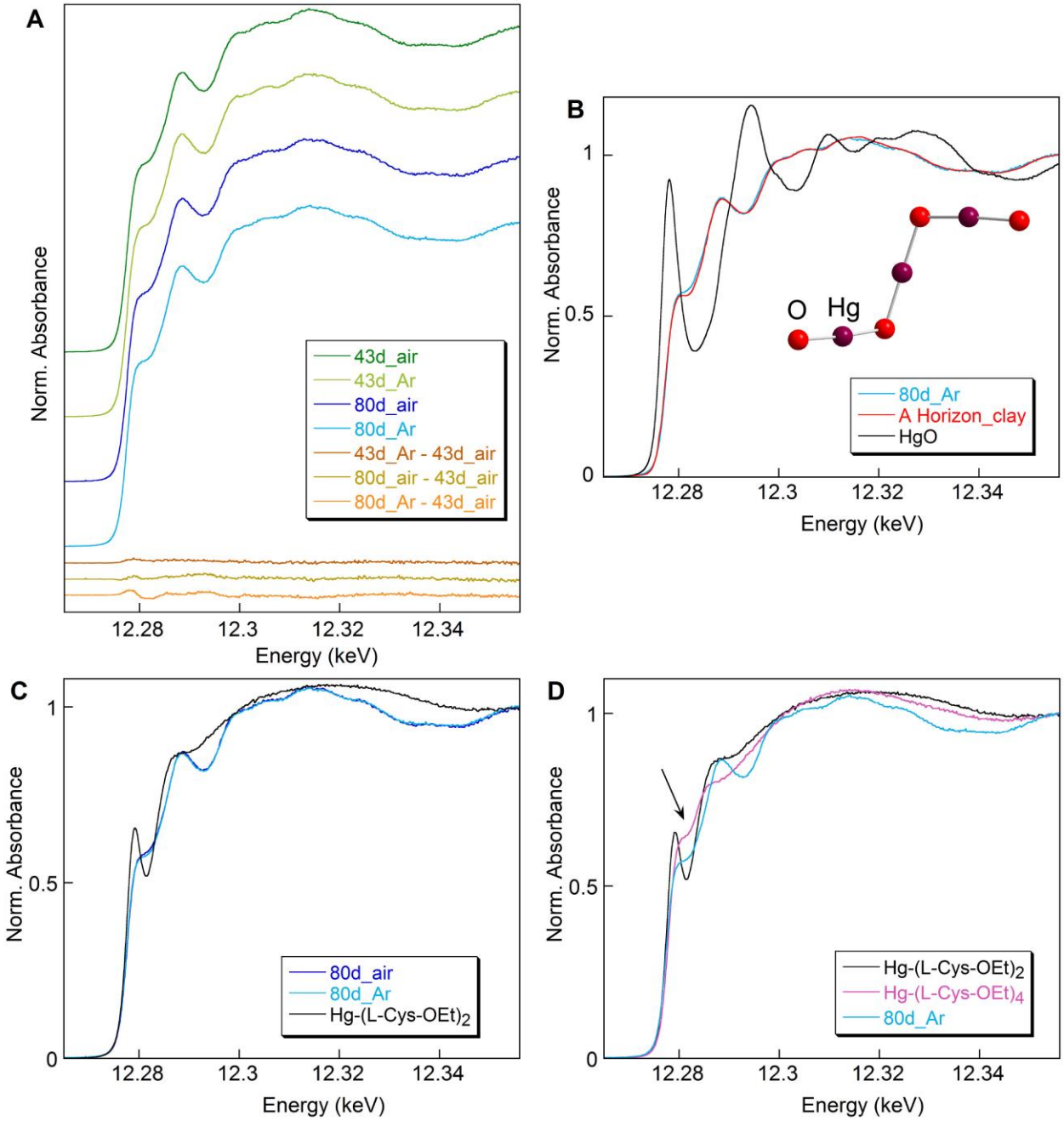

Fig. S7. (A) Comparison of the HR-XANES spectra for nanoparticulate β-HgS synthesized at room temperature (RT) from Hg-(L-Cys-OEt)$_2$ complexes aged for 43 and 80 days in contact with air or under

argon atmosphere. The similarity of the spectra is illustrated by the difference spectra shown at the bottom of the figure. (B) Plot showing the nearly identical spectra for the A horizon and synthetic nanoparticulate β-HgS, and their distinct differences from the HgO spectrum. HgO features Hg coordinated to two oxygens similar to monodentate and bidentate inner-sphere complexes on Al- and Fe-oxyhydroxides. (C, D) Plots showing that the nanoparticulate β-HgS reference has a distinct spectrum from the initial Hg-(L-Cys-OEt)$_2$ complex (C), and that its trace cannot be obtained by considering a change of Hg coordination to cysteinyl sulfur from 2-fold to 4-fold (D). In β-HgS, Hg is also coordinated to four sulfurs, but to sulfide ligands, which partly explains the observed differences with the Hg-(L-Cys-OEt)$_4$ complex. All spectra were recorded at 10 K (He-T).

1.2.2. Hg-SOM

The mercury-soil organic matter (Hg-SOM) compounds were prepared from a 0.1 mM $Hg(NO_3)_2$ stock solution in 0.01 M HNO_3 and Elliott Soil humic acid obtained from the International Humic Substances Society (IHSS; Cat. No. 1S102H; http://www.humicsubstances .org/). The humic acid had been isolated from Elliott Soil organic matter by high speed centrifugation to remove particles followed by repeated steps involving alkaline extraction (pH 12), high speed centrifugation, and precipitation at pH 1. Details of the procedure can be found at the IHSS web page. The ash content of the Elliot Soil HA is 0.88% when dry, consistent with the efficient removal of fine clays and biological cells. The ash-free dry weight composition is 58.13% C, 3.68% H, 34.08% O, 4.14% N, 0.44% S, and 0.24% P. Thiol sulfur comprises 18.4% of the total sulfur.[1]

Table S1. pH of aged suspensions of Hg-SOM between any two measurements and before re-adjustment to 6.

Sample								
15 hours	Time	0 h	15 h					
	Measured pH	6.05	6.04					
3 days	Time	0 h	15 h	3 d				
	Measured pH	5.92	-	5.82				
10 days	Time	0 h	6 d	7 d				
	Measured pH	6.05	6.12	6.15				
	Adjusted pH		5.98	5.96				
1 month	Time	0 h	1 d	22 d	30 d			
	Measured pH	5.98	6.04	6.51	5.88			
	Adjusted pH			6.02				
6 months	Time	0 h	38 d	66 d	94 d	122 d	155 d	165 d
	Measured pH	6.01	6.24	6.45	5.98	5.90	6.01	6.02
	Adjusted pH		6.08	6.03		6.00		

Aggregates of β–HgS nanocrystals could be imaged by TEM after six months (Fig. S8). They were difficult to observe, despite the high scattering power of Hg atoms, because of their small size and scarcity as a result of the low amount of Hg in the SOM (200 ppm), and the instability of the SOM matrix under the electron beam especially at high magnification. Observation was possible by depositing a single droplet of highly dispersed and diluted Hg-SOM on nonconventional TEM

grids (#01824; Ted Pella, Inc). The 400 mesh Cu grids are covered with standard holey carbon membrane coated with an ultrathin (~2 nm thick) plain carbon film to provide full support to the unstable SOM and β–HgS particles while reducing the undesired scattering from the C substrate in HRTEM imaging. Use of a diluted Hg-SOM solution on this grid limited SOM condensation under the beam. Positive identification of mercury sulfide by HRTEM comes from the high electron contrast observed in these grains and unambiguously from the lattice spacing determination. Their chemical composition could not be measured by nanoanalysis because the grains were too thin to give a measurable Hg X-ray line and the sample preparation too unstable at long exposure time. In addition, the Hg(Mα/β = 2191 – 2281 eV) X-ray peaks overlap with the S(Kα = 2309 eV) line,[9] and with the tail of the strong Cl(Kα = 2622 eV) peak from the SOM.

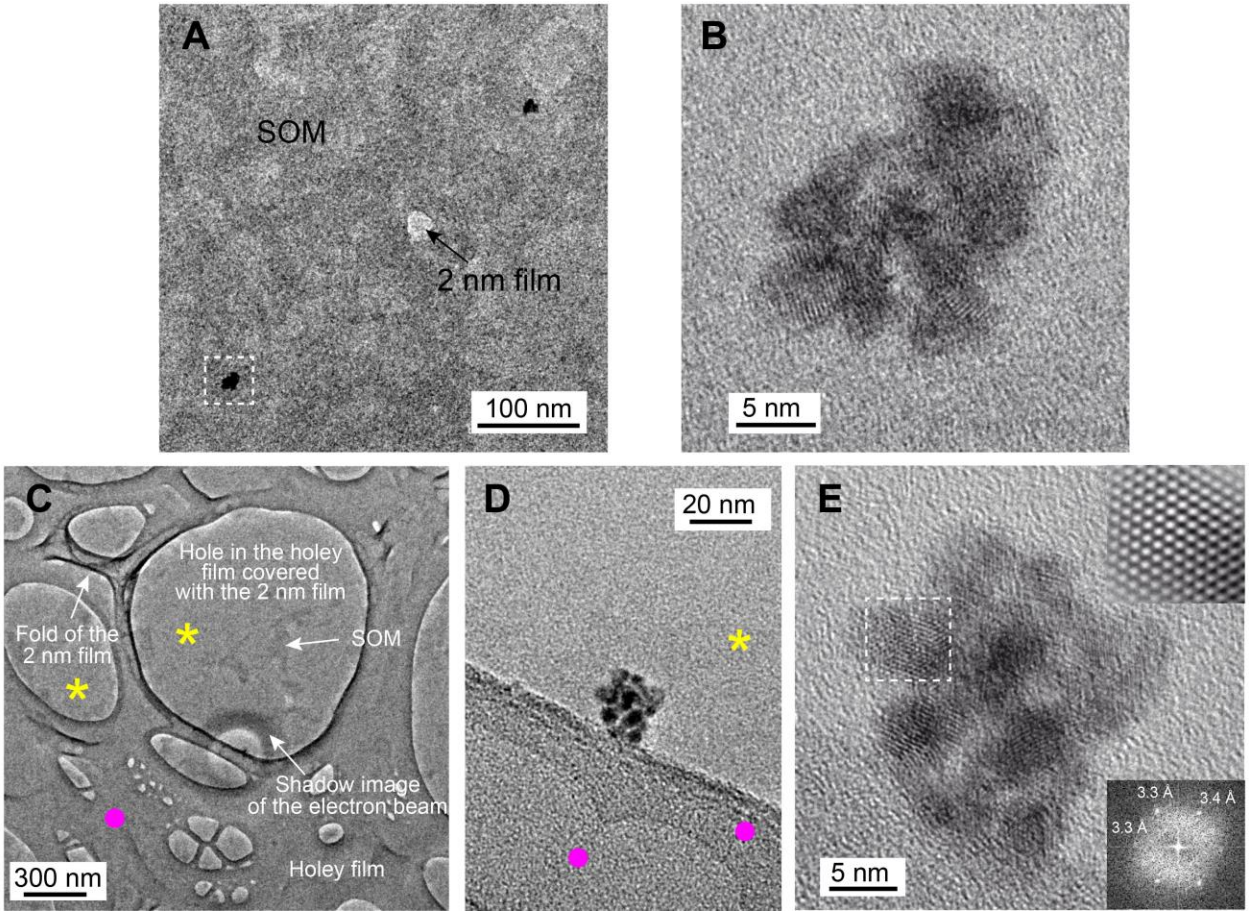

Fig. S8. HRTEM images of Hg-SOM on ultrathin (~2 nm) amorphous carbon membrane. (A) Two HgS aggregates (dark contrast) within a background of SOM (grey contrast). (B) High magnification image of the lower left aggregate in (A). This region contains relatively high amounts of SOM which decrease the contrast and hinder or limit the observation of lattice fringes. (C) Low magnification view of Hg-SOM on the ultrathin C film (yellow stars) covering a hole in the holey C membrane (pink circle). A small β-HgS aggregate is seen at the center of the shadow image of the condensed electron beam where the supporting ultrathin membrane contacts the underlying holey film. (D) Close-up view of the aggregate in (C). This region has less SOM, as evidenced by the enhanced contrast of the image. (E) High magnification image of the β-HgS aggregate and Fourier filtered image of a single grain (top right) with its FFT (lower right). The

FFT pattern is compatible with the <111> orientation of β-HgS crystals, as indicated by the close values of the three lattice plane spacings (3-fold symmetry).

1.3. Computational methods

1.3.1. Gibbs free energy calculations

Basis sets were chosen as follows: aug-cc-pVDZ functions[10] for the C and H centers, the aug-cc-pVTZ functions[11] for the S centers, and the Stuttgart-Dresden-Bonn (SDD) basis set[12] augmented by two polarization functions of type *f*[13] for the valence electrons of the Hg centers. The core electrons of Hg were frozen and represented using the SDD quasirelativistic pseudopotentials.[12]

1.3.2. Optimization of the $(RS\text{-}(Hg\text{-}S)_3\text{-}R)_3$ system

The size of the basis set was slightly reduced with respect to that used for the Gibbs free energy calculations by eliminating the two *f* functions added on the Hg centers. The calculations were performed using the density functional theory (DFT)[14] method with M06 potentials.[15]

2. Other examples of standard XANES vs. HR-XANES spectra

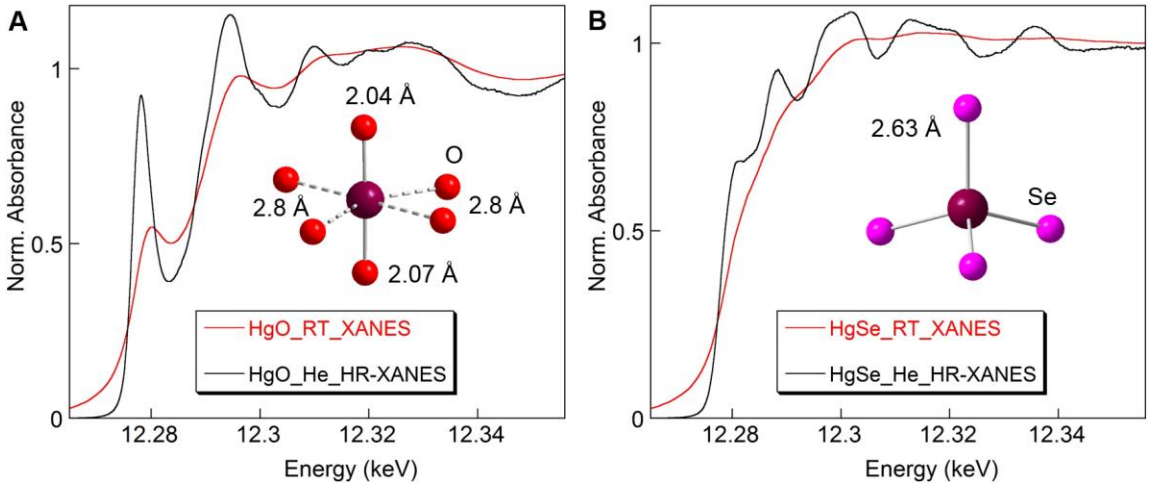

Fig. S9. Standard XANES spectra at room temperature (RT) and HR-XANES spectra at 10 K (He-T) of HgO and HgSe. (A) HgO has a chain structure, like α-HgS, with two short Hg-O bonds (2.04 – 2.07 Å) along the chain direction and four long Hg-O distances (2.8 Å) between chains.[16] (B) HgSe has a zincblende structure like β-HgS[17]. Linearly coordinated Hg(II) gives rise to a sharp peak which can be used to distinguish this coordination. This spectral feature is visible in HR-XANES because the intrinsic broadening of the L_3-edge XANES spectra is determined by the core hole lifetime of the $2p_{3/2}$ level in standard fluorescence experiment, which is as large as 5.5 eV,[18] and by the lifetime of the final $3d_{5/2}$ level, which is as narrow as 1-2 eV, in high-resolution mode.[19-22]

3. HR-XANES spectra of other reference compounds

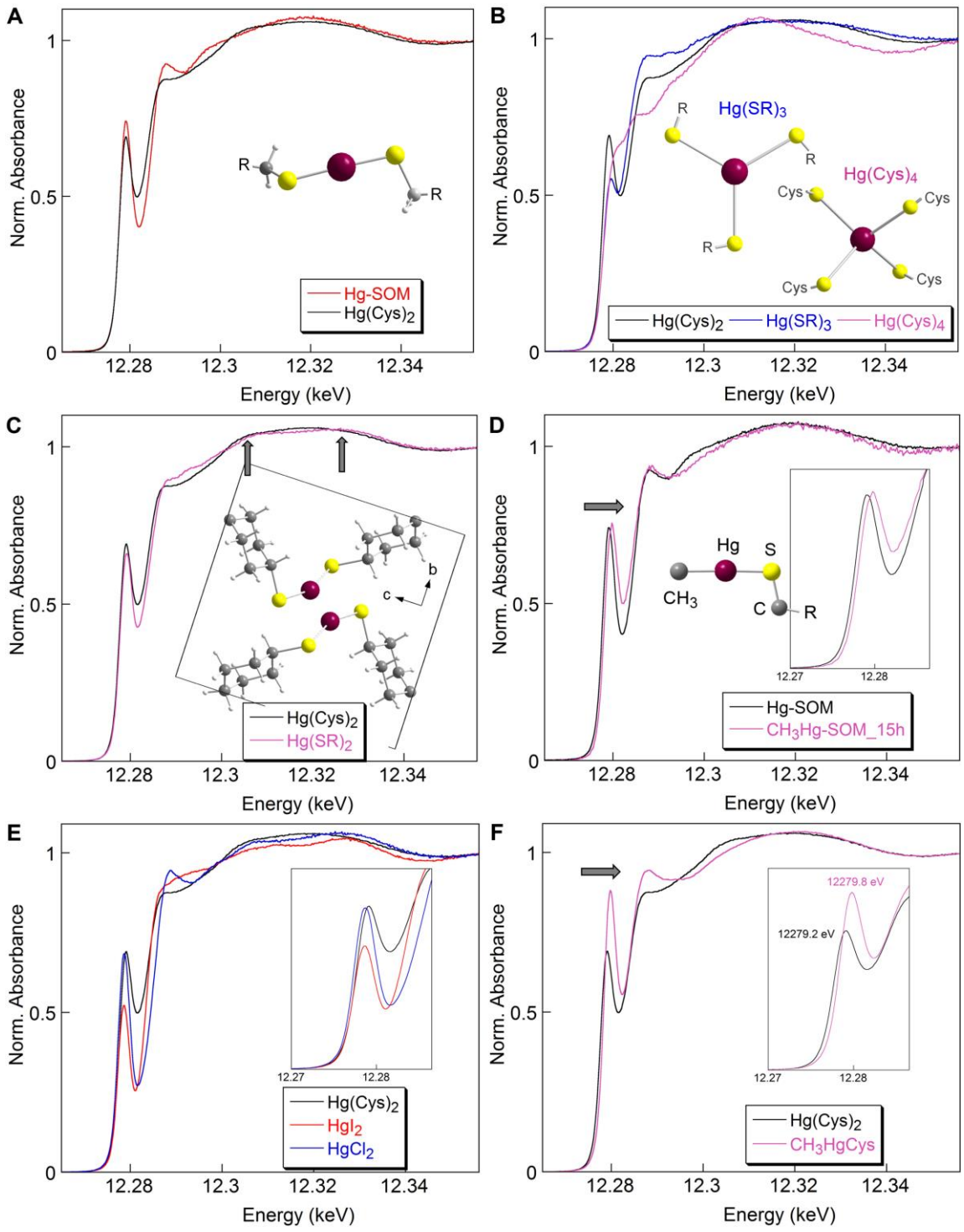
A
Norm. Absorbance
Energy (keV)
R
R
Hg-SOM
Hg(Cys)2
B
Hg(SR)3
Hg(Cys)4
Cys
Hg(Cys)2
Hg(SR)3
Hg(Cys)4
C
b
c
Hg(Cys)2
Hg(SR)2
D
Hg
S
CH3
C
R
Hg-SOM
CH3Hg-SOM_15h
E
HgI2
HgCl2
F
12279.8 eV
12279.2 eV
CH3HgCys

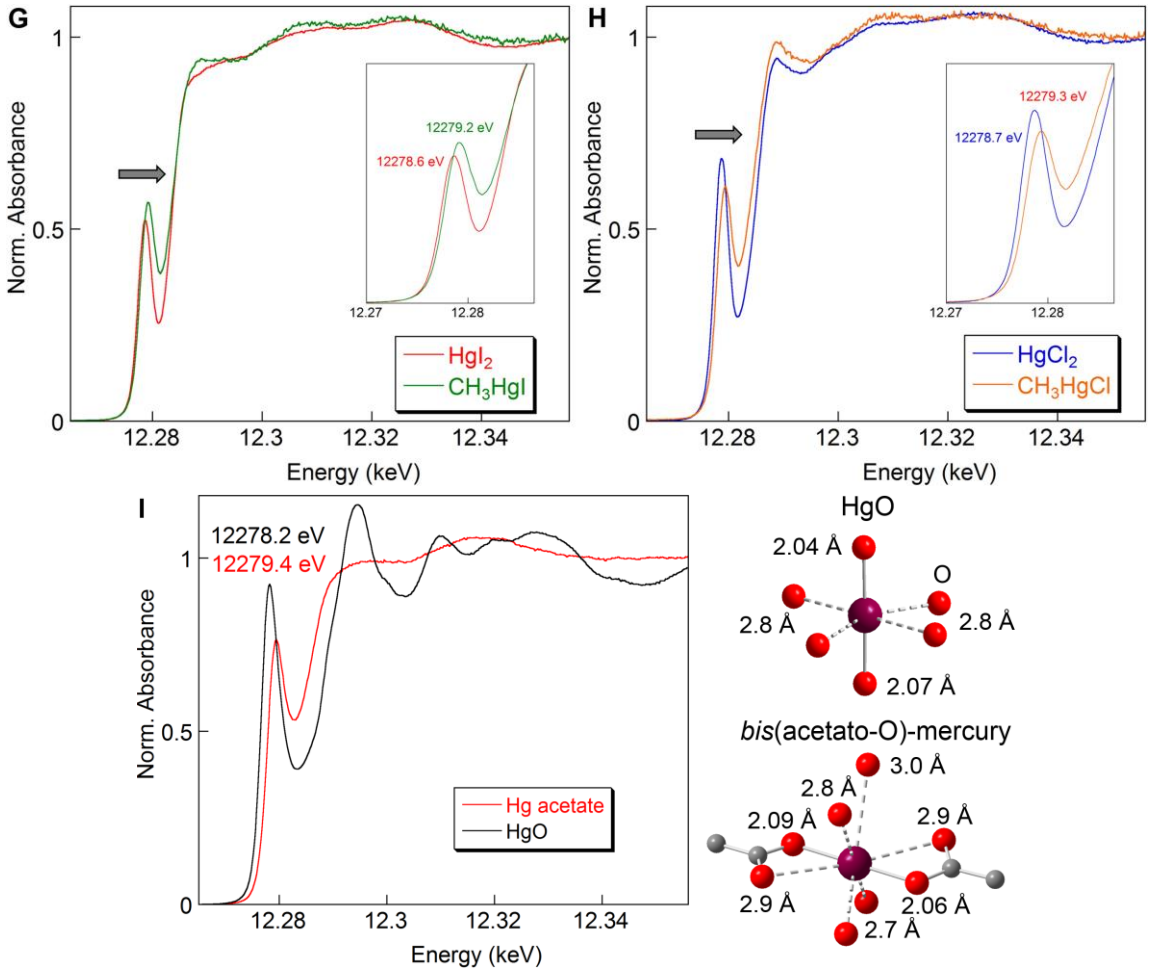

Fig. S10. HR-XANES spectra at 10 K (He-T) of Hg complexed to thiolate (RSH) groups (A-D) and bonded to iodine, chlorine, carbon (methyl) and oxygen ligands (E-I) showing the sensitivity of this technique to Hg speciation. (A) Hg linearly coordinated to two sulfurs at ~2.34 Å in Hg-SOM and Hg-(cysteine)$_2$, i.e., Hg(Cys)$_2$).[2, 23] The two spectra have features that differentiate the two binding environments beyond the first coordination shell. (B) Hg coordinated to three (Hg(SR)$_3$) and to four (Hg(Cys)$_4$) cysteinyl sulfurs. The change of coordination from two-fold to four-fold is accompanied by the disappearance of the sharp resonance at 12279 eV. The same phenomenon is observed for HgS_4 coordination in β-HgS (Fig. 1) and $HgSe_4$ coordination in HgSe (Fig. S9). The trigonal reference was synthesized after Alsina et al. (1992),[24] and the four-coordinate reference has been obtained at pH 8.4 with an excess of L-cysteine (Cys/Hg = 10).[23] (C) Digonal Hg coordinated to thiolate in solution (Hg(Cys)$_2$ complex formed at pH 8.4 and Cys/Hg = 2[23]) and in a crystal (Hg-cyclohexanethiolate complex[24]) showing that HR-XANES is sensitive to Hg-Hg pairs (arrows) in organic compounds, in addition to inorganic sulfides (Fig. 2C). (D-H) When Hg is digonally bonded to one methyl group and one sulfur, iodine or chlorine ligand, the resonance is consistently shifted to the right by 0.6 eV (arrows). (I) The crystallized *bis*(acetato-O)-Hg(II) molecule also has a chain structure closely related to that of HgO (and to a lesser degree to α-HgS), with two short Hg-O bonds (2.06-2.09 Å) along the chain direction.[25] Similarly to digonal Hg in thiolate complexes, the HR-XANES spectra for crystallized HgO and Hg acetate (HgAc) show a signature at ~12279 eV characteristic of linear coordination, but at higher energy reveal important structural differences because one compound is inorganic and the other organic. The resonance peaks at 12278.2 eV in HgO and 12279.40 in Hg acetate. This chemical shift is related to the ionic character of HgAc and semiconducting properties of HgO.[26, 27] The conduction band (approximated by the Lowest Unoccupied Molecular Orbital; LUMO) is lower for HgO, and the average bond length of HgO is correspondingly shorter by ~0.026 Å (<*d*(HgO)> = 2.053 Å;

<(*d*(HgAc)> = 2.079 Å). Thus, it takes less energy to promote the photoelectron to the conduction band, so the HgO edge feature is shifted to lower energy relative to HgAc.

4. Sensitivity of HR-XANES and standard XANES to Hg-SOM in a mixture with β-HgS

The sensitivity of high-resolution and standard resolution XANES to organically-bound Hg was estimated with synthetic mixtures of the well-crystallized β-HgS and Hg-SOM spectra. The well-defined absorption feature of Hg-SOM at 12279.2 eV observed in HR-XANES is seen clearly for a relative abundance of 15 mol% in a mixture with β-HgS (Fig. S11). The difference between the 15% Hg-SOM + 85% β-HgS spectrum and the 100% β-HgS spectrum has a normalized sum-squared residual $NSS = 6.1 \times 10^{-5}$. In contrast, the same synthetic mixture calculated with standard XANES data yields $NSS = 1.8 \times 10^{-5}$. The smaller difference between the pure β-HgS and the two-component spectra means lower spectral sensitivity to organically-bound Hg. Furthermore, standard XANES has a larger uncertainty of determination because the spectra for the two end-members are less different with this method. This effect can be estimated by calculating the weights of the standard XANES mixed spectra for which $NSS = 6.1 \times 10^{-5}$. The result is 28% Hg-SOM + 72% β-HgS. Note that the detection limit to organically-bound Hg that is achieved with XANES depends not only on the detection method, as demonstrated here, but also on the data quality and how well the standards represent the unknown sample (Fig. S12). The limit can be significantly better than 15% with HR-XANES if the fitted system is well-constrained by only two end-members, as in the case of the analysis of the kinetics series. In summary, the low-energy region of the Hg HR-XANES spectra, corresponding to electronic transitions to unoccupied 5*d* states, can be used to identify organically-bound Hg, whereas the high-energy region, corresponding to long scattering paths of the photoelectron, can be used as a fingerprint for long-distance Hg-Hg pairs within a cluster of Hg atoms.

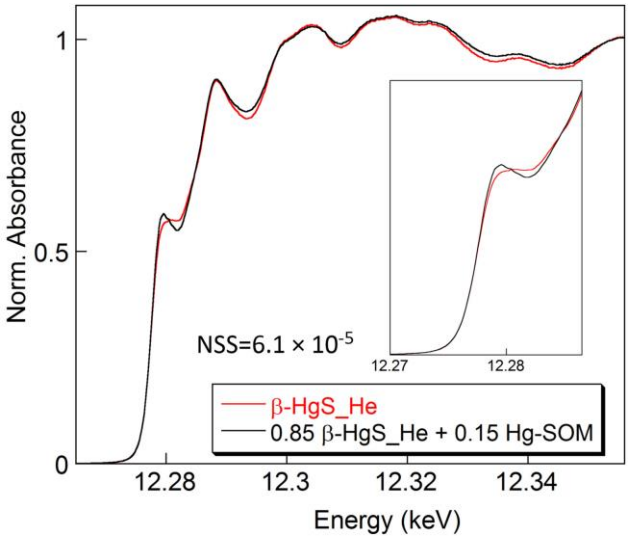

Fig. S11. Sensitivity of HR-XANES to the relative abundance of organically-bound Hg ($Hg(SR)_2$ complex) in a mixture with β-HgS.

5. HR-XANES spectra from the A horizon soil

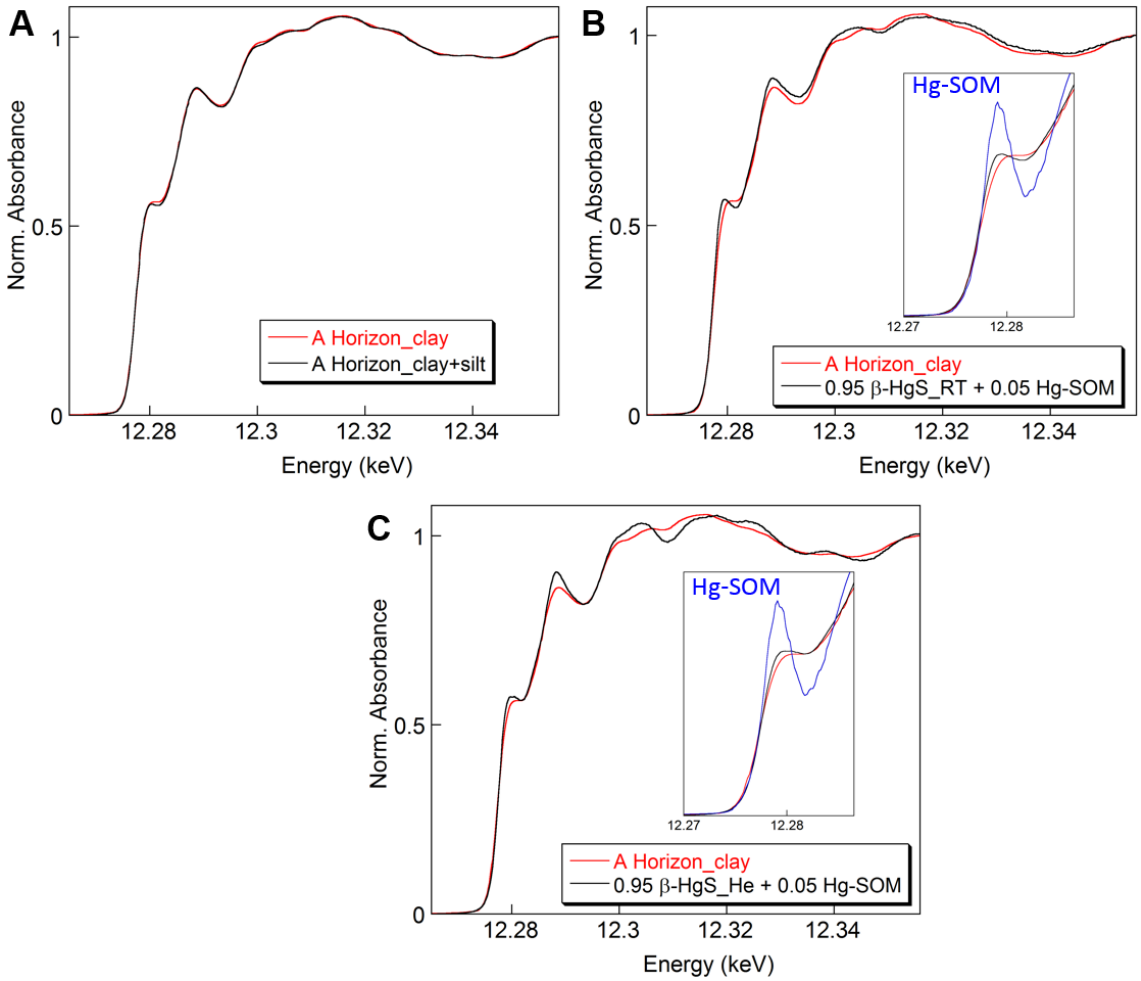

Fig. S12. (A) HR-XANES spectra at He-T of the clay-sized (0.1-2.0 μm) and clay and silt (2-63 μm) fractions from the A horizon. The two spectra are statistically indistinguishable, which we interpret to indicate that the β-HgS nanoparticles are aggregated, as observed by TEM (Fig. S8) and is typically the case for nanosized minerals in soils and sediments.[28] (B,C) Comparison of the A horizon clay spectrum at He-T with the spectra for a mixture of 95% well-crystallized β-HgS (RT or He-T) and 5% Hg-SOM (He-T) indicates that the organically-bound fraction in the A horizon makes up < 5% of Hg total. The two insets show the diagnostic feature at 12279.2 eV used to detect the Hg-SOM component. The similarity of the clay spectrum and clay plus silt spectrum provides further evidence against detectable Hg-SOM otherwise its proportion would be expected to vary with the sample fraction size.

6. Precision on the fractions of β-HgS and Hg-SOM in the O horizon soil

The precision on the fractions of β-HgS and Hg-SOM derived from the fitting of the O horizon spectrum (Fig. 2D) was evaluated by progressively increasing the proportion of one component at fixed values different from the best-fit value (74% and 26%, respectively) and optimizing the proportion of the other component. The fit was clearly degraded for a 10% increase of the best-fit residual (normalized sum-squared residual, *NSS*). This process leads to an uncertainty range of ± 6 mol% of total Hg for each species. The proportion of α-HgS obtained by adding this species to the β-HgS + Hg-SOM two-component fit was 5% and *NSS* decreased by 6%, which is within

experimental noise. If present, cinnabar is a minor species in the O horizon and in Hg-SOM aged for six months (Fig. 2D).

7. References for the Supporting information

(1) Manceau, A.; Nagy, K. L., Quantitative analysis of sulfur functional groups in natural organic matter by XANES spectroscopy. *Geochim. Cosmochim. Acta* **2012,** *99*, 206-223.

(2) Nagy, K. L.; Manceau, A.; Gasper, J. D.; Ryan, J. N.; Aiken, G. R., Metallothionein-like multinuclear clusters of mercury(II) and sulfur in peat. *Environ. Sci. Technol.* **2011,** *45*, 7298–7306.

(3) Patriarche, G.; Walter, P.; Van Eslandre, E.; Ayache, J.; Castaing, J., Characteristics of HgS nanoparticles formed in hair by a chemical reaction. *Phil. Mag.* **2013,** *93*, 137–151.

(4) Rodic, D.; Spasojevic, V.; Bajorek, A.; Onnerud, P., Similarity of structure properties of $Hg_{1-x}Mn_xS$ and $Cd_{1-x}Mn_xS$ (structure properties of HgMnS and CdMnS). *J. Mag. Mag. Mater.* **1996,** *152*, 159-164.

(5) Wang, H.; Zhu, J. J., A sonochemical method for the selective synthesis of α-HgS and β-HgS nanoparticles. *Ultrason. Sonochem.* **2004,** *11*, 293–300.

(6) Lebail, A.; Duroy, H.; Fourquet, J. L., Ab-initio structure determination of $LiSbWO_6$ by X-ray powder diffraction. *Mater. Res. Bull.* **1988,** *23*, 447-452.

(7) Rodríguez-Carvajal, J., Recent developments of the program FULLPROF. *Commission on powder diffraction (IUCr). Newsletter* **2001,** *26*, 12-19.

(8) Neville, G. A.; Berlin, M., Mercury(II) complexes of L-cysteine methyl-ester. *Can. J. Chem.* **1973,** *51*, 3970-3974.

(9) Deonarine, A.; Hsu-Kim, H., Precipitation of mercuric sulfide nanoparticles in NOM-containing water: Implications for the natural environment. *Environ. Sci. Technol.* **2009,** *43*, 2368–2373.

(10) Dunning, T. H., Gaussian-baisis sets for use in correlated molecular calculations. 1. The atoms boron through neon and hydrogen. *J. Chem. Phys.* **1989,** *90*, 1007-1023.

(11) Woon, D. E.; Dunning, T. H., Gaussian-basis sets for use in correlated molecular calculations. 3. The atoms aluminum through argon. *J. Chem. Phys.* **1993,** *98*, 1358-1371.

(12) Andrae, D.; Haussermann, U.; Dolg, M.; Stoll, H.; Preuss, H., Energy-adjusted *ab initio* pseudopotentials for the second and third row transition-elements. *Theor. Chim. Acta* **1990,** *77*, 123-141.

(13) Martin, J. M. L.; Sundermann, A., Correlation consistent valence basis sets for use with the Stuttgart-Dresden-Bonn relativistic effective core potentials: The atoms Ga-Kr and In-Xe. *J. Chem. Phys.* **2001,** *114*, 3408-3420.

(14) Kohn, W.; Sham, L. J., Self-consistent equations including exchange and coreelation effects. *Phys. Rev. A* **1965,** *140*, 1133-1138.

(15) Zhao, Y.; Truhlar, D. G., The M06 suite of density functionals for main group thermochemistry, thermochemical kinetics, noncovalent interactions, excited states, and transition elements: two new functionals and systematic testing of four M06-class functionals and 12 other functionals. *Theor. Chem. Acc.* **2008,** *120*, 215-241.

(16) Aurivillius, K., Least-squares refinement of the crystal structures of orthorhombic HgO and of Hg_2O_2NaI. *Acta Chem. Scand.* **1964,** *18*, 1305-1306.

(17) Cardona, M.; Kremer, R. K.; Lauck, R.; Siegle, G.; Munoz, A.; Romero, A. H., Electronic, vibrational, and thermodynamic properties of metacinnabar β-HgS, HgSe, and HgTe. *Phys. Rev. B* **2009,** *80*, 195204

(18) Krause, M. O.; Oliver, J. H., Natural widths of atomic *K* and *L* levels, *Kα* X-ray lines and several *KLL* Auger lines. *J. Phys. Chem. Ref. Data* **1979,** *8*, 329-338.

(19) Hämäläinen, K.; Siddons, D. P.; Hastings, J. B.; Berman, L. E., Elimination of the inner-shell lifetime broadening in X-ray-absorption spectroscopy. *Phys. Rev. Lett.* **1991,** *67*, 2850-2853.

(20) de Groot, F. M. F.; Kotani, A., *Core Level Spectroscopy of Solids*. Taylor and Francis: New York, 2008.

(21) Glatzel, P.; Weng, T. C.; Kvashnina, K.; Swarbrick, J.; Sikora, M.; Gallo, E.; Smolentsev, N.; Mori, R. A., Reflections on hard X-ray photon-in/photon-out spectroscopy for electronic structure studies. *J. Elec. Spec. Relat. Phenom.* **2013,** *188*, 17-25.

(22) Rovezzi, M.; Glatzel, P., Hard X-ray emission spectroscopy: a powerful tool for the characterization of magnetic semiconductors. *Semicond. Sci. Technol.* **2014,** *29*, 023002.

(23) Jalilehvand, F.; Leung, B. O.; Izadifard, M.; Damian, E., Mercury(II) cysteine complexes in alkaline aqueous solution. *Inorg. Chem.* **2006,** *45*, 66-73.

(24) Alsina, T.; Clegg, W.; Fraser, K. A.; Sola, J., Homoleptic cyclohexanethiolato complexes of mercury(II). *J. Chem. Soc. Dalton Trans.* **1992,** *8*, 1393-1399.

(25) Allmann, R., Structure of mercuric acetate. *Zeit. Krist.* **1973,** *138*, 366-373.

(26) Biering, S.; Hermann, A.; Furthmuller, J.; Schwerdtfeger, P., The unusual solid-state structure of mercury oxide: Relativistic density functional calculations for the group 12 oxides ZnO, CdO, and HgO. *J. Phys. Chem. A* **2009,** *113*, 12427-12432.

(27) Glans, P. A.; Learmonth, T.; Smith, K. E.; Guo, J.; Walsh, A.; Watson, G. W.; Terzi, F.; Egdell, R. G., Experimental and theoretical study of the electronic structure of HgO and Tl_2O_3. *Phys. Rev. B* **2005,** *71*, 235109.

(28) Manceau, A.; Nagy, K. L.; Marcus, M. A.; Lanson, M.; Geoffroy, N.; Jacquet, T.; Kirpichtchikova, T., Formation of metallic copper nanoparticles at the soil-root interface. *Environ. Sci. Technol.* **2008,** *42*, 1766-1772.